A Three-State Model for Connexin37 Gating Kinetics

S. V. Ramanan,* P. R. Brink,* K. Varadaraj,* E. Peterson,* K. Schirrmacher,# and K. Banach*
*Department of Physiology and Biophysics, State University of New York at Stony Brook, Stony Brook, New York 11794-8661 USA, and #Institut für Physiologie, Universität-GH Essen, D-45122 Essen, Germany

ABSTRACT The gating behavior of human connexin 37 (hCx37) is unaffected by the nature of the bathing monovalent (for Na, K, Rb). It is modified by [Mg] in the millimolar range. For fitting the kinetics, we propose a simple extension to three states of the canonical 2-state model of the hemichannel. The extra closed state allows for some immobilization of a hemichannel at high transjunctional voltages. The model is reasonably efficient at fitting data at various voltage protocols. Interpreting the fits of the data at different [Mg] is consistent with a binding site for Mg.

INTRODUCTION

Gap junction channels are a conduit for direct intercellular communication, providing as they do a permeable pore for ions and small macromolecules. Each gap junction channel is composed of two hemichannels, with one hemichannel contributed by each of the two cells that form a coupled pair. Each hemichannel, in turn, is formed by six subunits, the connexins. A hemichannel that is composed of identical connexins is referred to as a homotypic hemichannel and has a sixfold symmetry axis (Makowski, 1988; Yeager and Nicholson, 1996). The homotypic gap junctions that are studied here are composed of human connexin 37 (hCx37). Of all homotypic gap junctions, the Cx37 channel has the largest conductance, ~370 pS in 135 mM KCl (Veenstra et al., 1994). The Cx37 channel also gates away from the open state at low transjunctional potentials. Macroscopically, there is a component of the conductance that falls off as a Boltzmann against transjunctional voltage V_j, albeit not to zero. The Boltzmann is centered at a V_0 of ~25–30 mV (Brink et al., 1997; Veenstra et al., 1994).

In this study, we examined the gating properties of the hCx37 channel. The data and analysis provide evidence for an additional closed state for the hCx37 hemichannel, with slow and fairly voltage-insensitive kinetics (of the order of seconds and a charge of ~½ *e*) for the transitions to and from this state.

MATERIALS AND METHODS

Neuroblastoma cells (N2a) transfected with cDNA for hCx37 were used in all of the experiments described here. The cell line was the same as that used by Brink et al. (1997). All experiments were performed by the double whole-cell patch-clamp technique (DWCP) (Neyton and Trautmann, 1985). The pipette solutions that were used in the experiments contained (in mM) 180 RbCl, NaCl, CsCl, or KCl; 1 $CaCl_2$; 1 EGTA; 1.8 $MgCl_2$; 10 HEPES (pH 7.1). Sometimes an equal mixture of KCl and NaCl was used, still at a total salt concentration of 180 mM. The bathing solution contained (in mM) 180 CsCl; 1 $CaCl_2$; 1.8 $MgCl_2$; 10 HEPES (pH 7.1–7.3). In some experiments the pipette and external bathing media contained 110 mM KCl rather than 180 mM.

Single and multichannel (microscopic) data were collected and analyzed as described by Brink et al. (1996). Briefly, the data were stored directly on videotape and reacquired with a 16-bit A/D converter. Macroscopic data were collected with the LabMaster board (Scientific Instruments) and the pClamp software system (Axon Instruments).

All of the records that have been analyzed were obtained by stepping one cell to various holding potentials while holding the other cell at 0 mV. Before this, the offset potentials on the patch-clamp amplifiers were adjusted so that both amplifiers passed zero current at an apparent holding potential of 0 mV. The records that are analyzed here were all taken from the cell held at 0 mV. To avoid the problems associated with series resistance in high-conductance pairs (Wilders and Jongsma, 1992), we have not studied data sets where the apparent junctional resistance was less than 50 MΩ in 110 mM KCl solutions, which is 10–25 times the pipette resistance in solution (~2–5 MΩ). This puts an upper limit of ~50 Cx37 channels on all of the macroscopic records shown here.

RESULTS

General characteristics of gating

Fig. 1 *a* shows a typical macroscopic record from a coupled pair (17 nS). Both pipettes contained 110 mM KCl and 1.8 mM $MgCl_2$. A +10 mV prepulse lasting 1 s is followed by steps to various junctional potentials from −150 mV to 150 mV in steps of 20 mV for 4 s. This step is followed by a step of the opposing polarity for another 4 s. As noted by Nicholson et al. (1993) and Reed et al. (1993), deactivation of the Cx37 channel has a multiexponential time course, with a fast component that, in these records, is more voltage-dependent than the slower component. Reversing the voltage polarity invariably produces instantaneous current peaks that are smaller than the current peaks generated by steps directly from 0 mV. This is more clearly illustrated in Fig. 1 *b*, where the steps are 400 ms long, but the time resolution is better (1 ms, also from the experiment in Fig. 1 *a*). The presence of a second, slower component in the kinetics is evident, even in these smaller time frames.

Received for publication 25 November 1997 and in final form 25 February 1999.

Address reprint requests to Dr. Peter R. Brink, Department of Physiology and Biophysics, SUNY Health Sciences Center, State University of New York at Stony Brook, Stony Brook, NY 11794-8661. Tel.: 516-444-3124; Fax: 516-444-3432; E-mail: peter@patch.pnb.sunysb.edu.

0006-3495/99/05/2520/10 $2.00

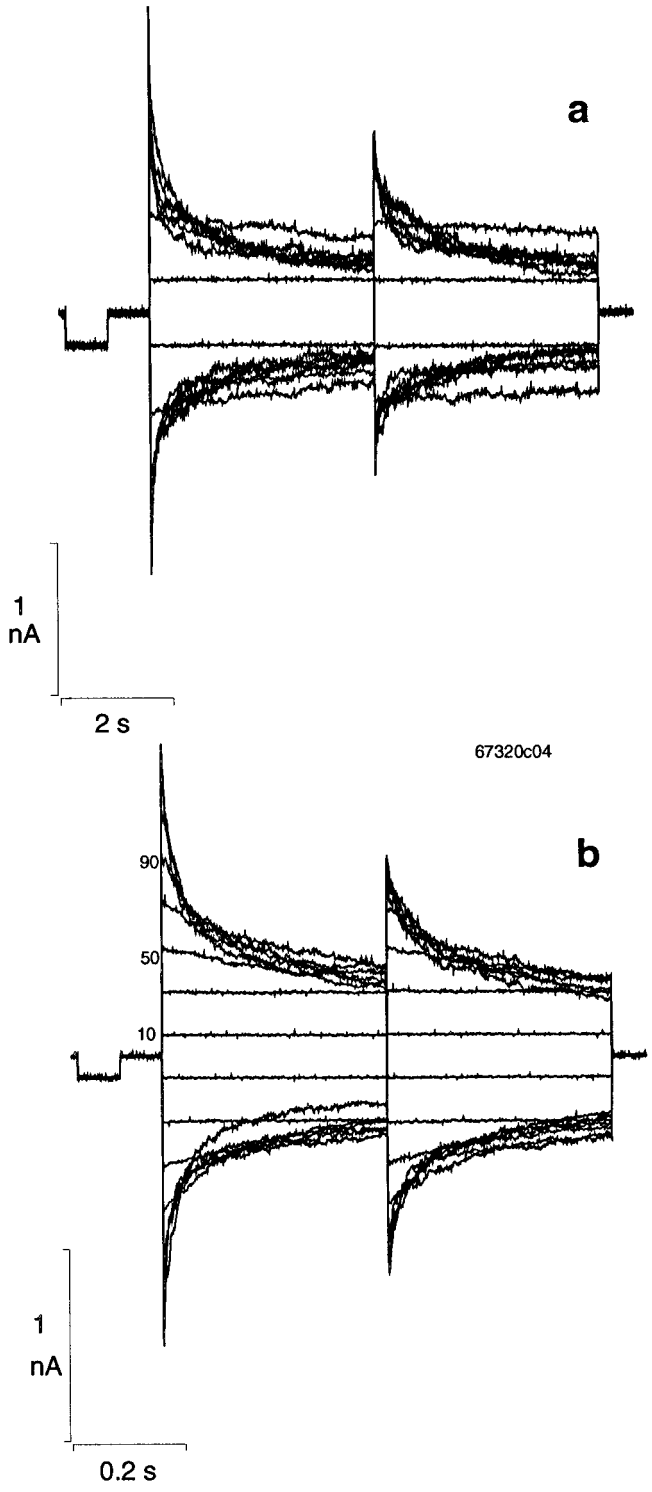

FIGURE 1 Data from the recipient cell of a double whole-cell patch recording. The pipettes contained 110 mM KCl and 1.8 mM $MgCl_2$. The protocols in the two panels are identical except for the time scale. After a test step (used for normalization) to 10 mV, the potential was stepped in the range from −150 mV to 150 mV in steps of 20 mV. After 4 s in *a* and 400 ms in *b*, the potential was inverted. Note the presence of two time constants in the relaxation to steady state. The two records are from the same patch.

Gating is indifferent to the nature of the cation

Fig. 2 is a plot of the normalized conductance G, 4 s after the onset of the voltage step, against the junctional voltage V_j, from macroscopic records. Both pipettes contained 180 mM of the monovalent (KCl, RbCl, or NaCl) and 1.8 mM of $MgCl_2$. The data were normalized to the maximum conductance observed, which was always at the smallest potential imposed, usually ±10 mV. It would seem that, regardless of the cation, the G–V_j records are very similar. The gating of hCx37 appears to be unaffected by the monovalent cation type. The average of all of the records was fitted by the conventional model that assumes two gates in series, with each gate sensing the applied voltage independently, i.e., by an equation of the form

$$G(V_j) - G_{min} = (G(0) - G_{min}) \frac{(1 + e^{AV_0})^2}{(1 + e^{-A(V-V_0)})(1 + e^{-A(-V-V_0)})} \quad (1)$$

Here $G(V)$ is the conductance at transjunctional voltage V_j, the parameter A is related to the steepness of activation, and G_{min} is the residual conductance at large V_j. The values of the best-fit parameters (least square fit) were $G_{min}/G(0) = 0.11$, $A = 0.078$ ($z = 2$), $V_0 = 21$ mV.

Microscopic gating data

Fig. 3 *a* shows a portion of a single-channel record from the recipient cell (held at 0 mV) with a junctional potential V_j = 20 mV. The pipettes contained 180 mM CsCl and 1.8 mM $MgCl_2$. If two channels were present in the patch, there would be a finite probability (see next paragraph) that they would open simultaneously; however, no double openings

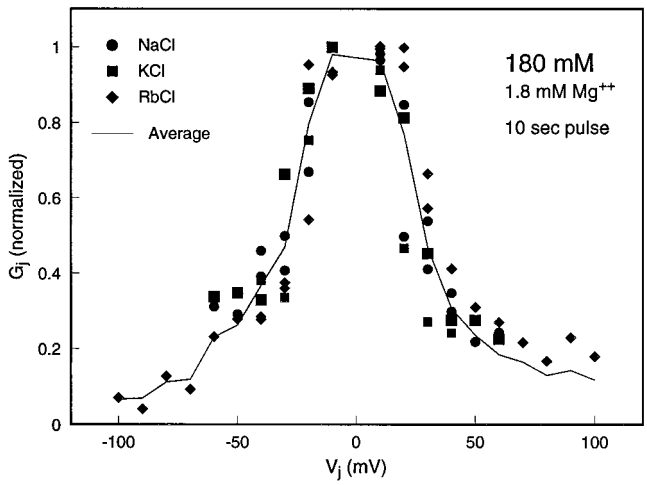

FIGURE 2 Conductance G at the end of a 4-s step plotted against the transjunctional potential V_j. The pipette contained 180 mM of the monovalent chloride salt XCl (X = Na, K, or Rb). The smooth line is the average over the various data sets. The G–V curve seems indifferent to the nature of the monovalent. Parameters for a Boltzmann fit to the data (not shown) are given in the text.

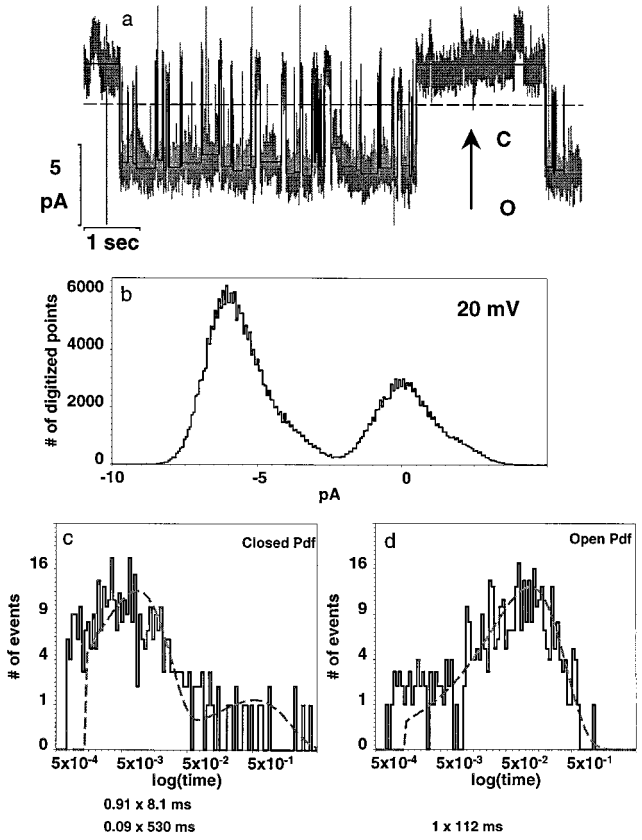

FIGURE 3 (*a*) A recording from a single Cx37 channel with both patch pipettes containing 180 mM KCl and 1.8 mM $MgCl_2$. The amplitude histogram of the entire 64 s of the record at $V_j = 20$ mV is shown in *b*. The data were idealized according to the half-amplitude criterion. Pdf's of the closed and open times and fits to exponentials are shown in *c* and *d*, respectively, in a Sigworth-Sine plot. Parameters for the fits are given in the text.

were seen for the duration of the recording, namely for 64 s. Fig. 3 *b* shows the amplitude histogram of the entire record. This data set is one of five experiments in which a single channel was observed.

All gap junction channels that have been documented at the single-channel level share the property of possessing at least one substate, and often many more. Cx37 shares this peculiar characteristic; moreover, it rarely shuts to the zero-current level. Instead, the channel shuts to a substate with a conductance that is ~¼ of the maximum conductance, in which it remains quiescent for extended intervals. Because closures to zero current are very infrequent, the discriminator for idealization of the trace was set half-way between the open and substate currents. Idealization of the record according to the half-amplitude criterion (Colquhoun and Sigworth, 1983) yields statistics on the probability density functions (pdf's) of the open and closed times and corresponding errors (Dabrowski and McDonald, 1992). Examination of these statistics by standard methods (same references) yields a probability of 6×10^{-12} that there were two channels in the record and that no simultaneous openings were seen. We will therefore assume that all activity in the record arose from the activity of one channel.

Fig. 3 *c* shows the distributions of closed-time pdf's in a Sigworth-Sine plot (Sigworth and Sine, 1987). The closed pdf (391 sojourns) is fitted by two well-separated exponentials, one with a time constant $\tau = 8$ ms and the other with $\tau = 530$ ms. Fig. 3 *d* shows the pdf's of open times; this is well fit by one exponential with $\tau = 112$ ms.

Fig. 4 *a* shows the two closed-time constants and the open-time constant from five different patches in the range $15 \leq |V| \leq 25$ mV. Because the gating seems insensitive to the particular cation, we have merged results from the analysis of patches containing only one channel with solutions containing different cations (all at 180 mM XCl, where X is K, Na, or an equal mixture of Na and K). The rate

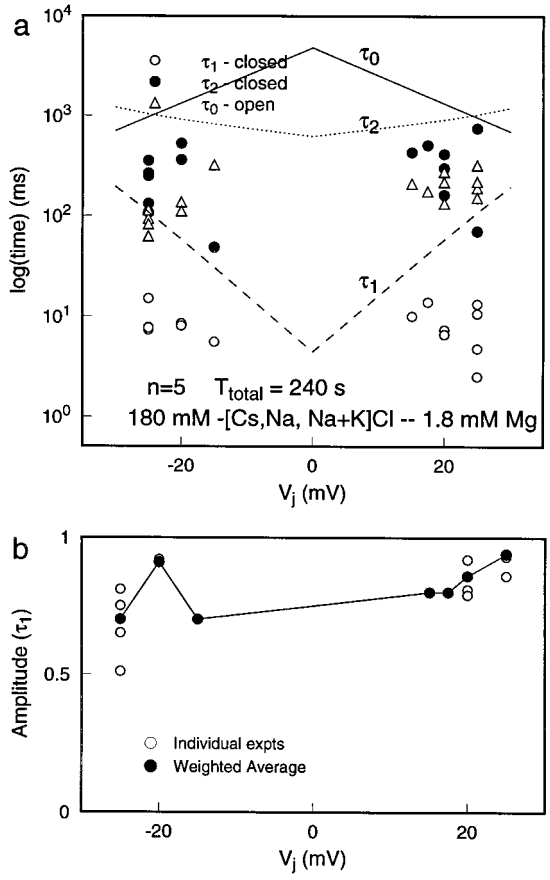

FIGURE 4 Time constants for fits to closed and open pdf's as in Fig. 3, *c* and *d*, are plotted against transjunctional voltage in *a*. Because the channel gating seems to be unaffected by the monovalent (see Fig. 2), data from experiments with different salts are pooled in this plot. All experiments are with 180 mM of the monovalent and 1.8 mM $MgCl_2$. In *a*, the open and filled circles are the short and long closed time constants, respectively, and the triangles represent the open time constant. The weight of the fast time constant in the closed pdf is plotted in *b*. Both the weight and the individual time constants seem not to depend on the voltage in the range plotted. The lines in *a* are the prediction from the model for the time constants (parameters from Table 1). The solid line and the long dashed line are the predictions for the long and short closed time constants, and the short dashed line is the prediction for the mean single-channel open time.

constants do not seem to be very dependent on voltage in the range examined, namely from 15 to 25 mV. Fig. 4 *b* shows the weights of the two closed rate constants on voltage; again they do not seem to vary much with applied potential in the tested range. In sum, five patches at 17 holding potentials with a total of 1469 (closed or open) sojourns were used in generating the data shown in Fig. 4.

In the single-channel pdf analysis presented so far, we have excluded all of the long closures characteristic of the Cx37 channel (Veenstra et al., 1994). These closures are present even at small junctional potentials and dominate the gating profile at high V_j's. The duration of these long closures varies from a few seconds (5–15) at small V_j's to many minutes at potentials greater than ~40 mV. Consequently, we have been unable to collect enough meaningful statistics on their frequency and duration.

Effects of Mg^{2+} on gating

Fig. 5, *a* and *b*, show normalized data with 110 mM KCl at 10 mM and 0.08 mM $MgCl_2$, respectively, in 1-s records. It

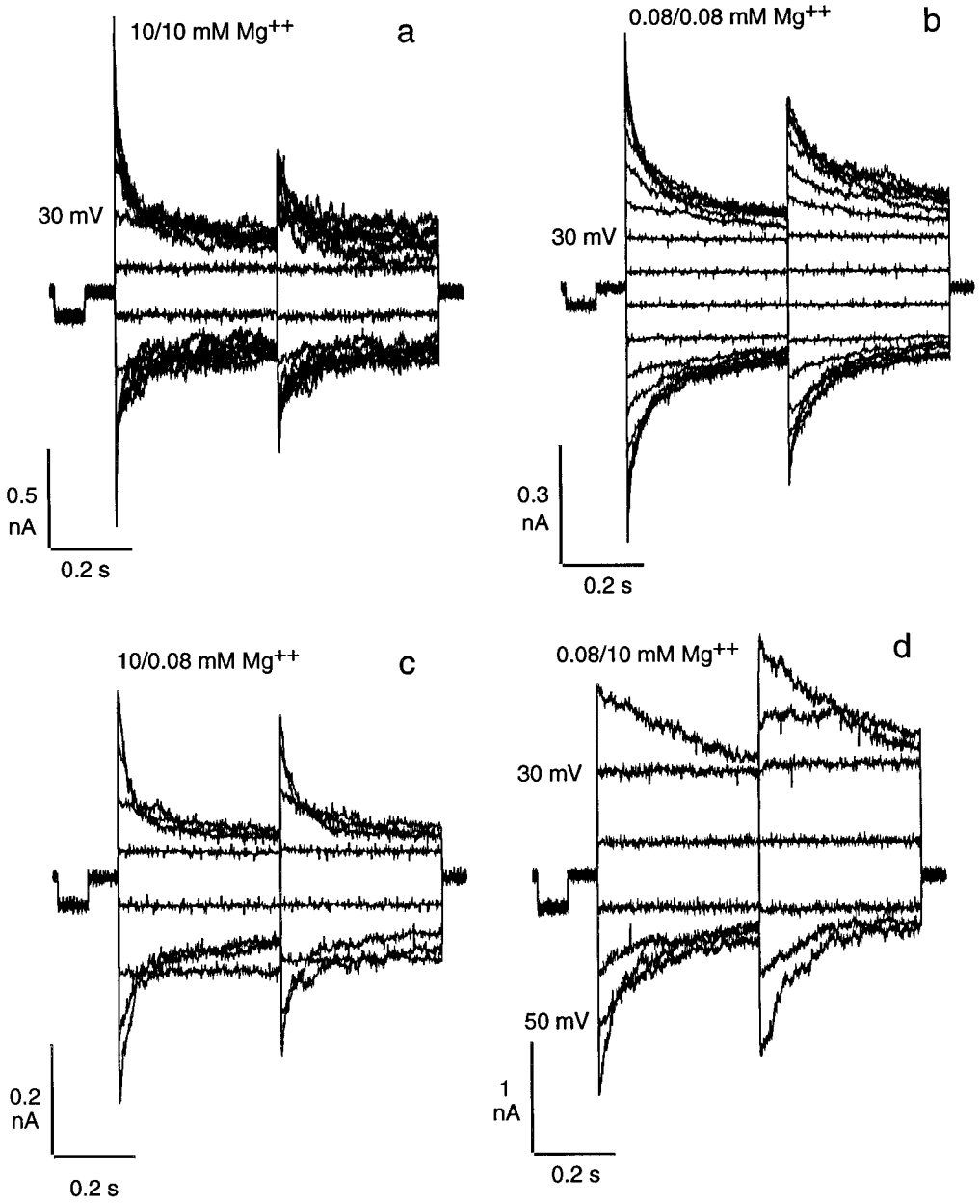

FIGURE 5 Dependence of Cx37 gating on magnesium concentration. All panels show data sets of 1 s duration collected with the same protocol as in Fig. 1, and with 110 mM KCl in the pipette. *a* and *b* are from recordings, where both pipettes had 10 mM and 0.08 mM $MgCl_2$, respectively. *c* is from a recording where one of the patch pipettes (the recipient) had 0.08 mM and the other (stepped) pipette had 10 mM $MgCl_2$, and in *d* the $MgCl_2$ concentrations in the stepped and recipient cells are reversed from *c*. The presence of Mg^{2+} apparently modulates the voltage inactivation in a fashion that is most clearly seen at a V_j of 30 mV.

would appear that changing the Mg^{2+} concentration has a pronounced influence on the kinetics at 400-ms step durations. This is especially visible in the current responses at a V_j of 30 mV, where the 0.08 mM Mg^{2+} pair is very insensitive compared to the deactivation observed when the Mg^{2+} concentration is 10 mM. In all experiments where the 0.08 mM Mg^{2+} pipette solution was used, this effect was observed (five patches at 110 mM KCl and 0.08 mM $MgCl_2$; four patches at 110 mM KCl and 10 mM $MgCl_2$).

To ensure that this effect of Mg^{2+} did not arise from artifacts, data were collected from pairs where one pipette had 10 mM $MgCl_2$ and the other had 0.08 mM $MgCl_2$ (Fig. 5, *c* and *d*, two different cell pairs). Such data display a pronounced asymmetry, with kinetics that resembles the records from the 10 mM Mg^{2+} pair of Fig. 5 *a* when the 10 mM Mg^{2+} cell is stepped positive. Similarly, the kinetics of the asymmetrical Mg^{2+} records in Fig. 5, *c* and *d*, resemble the low-Mg^{2+} (0.08 mM) record when the low-Mg^{2+} cell is stepped positive. The data shown are consistent with the positive cytoplasmic polarity assigned to Cx37 hemichannel voltage gating in the homotypic configuration (White et al., 1994). In all of the macroscopic experiments with asymmetrical Mg^{2+} ($n = 4$ with 10 mM/0.08 mM; $n = 10$ with 1.8/0.08 mM), similar asymmetry was observed.

Substate gating

At elevated salt concentrations (270 mM KCl at V_j of 40 mV; Fig. 6) or at high transjunctional voltages (data not shown; $V_j \geq 100$ mV), records in low-conductance pairs show transitions from the subconductance to the completely closed state. Moreover, many of these transitions seem to be fast enough to appear instantaneous when the data are reacquired at a low-pass filter setting of 1 kHz and sampled at 50 μs. Residual states thought to be distinctly different from other subconducting states in gap junction channels by virtue of their slower gating kinetics to the ground state or $I_j = 0$ pA have been reported (Bukauskas and Weingart, 1993). These data do not contradict the slow transitions but clearly show that rapid transitions to the closed state occur.

A SIMPLE MODEL OF CHANNEL GATING

The pdf's for the closed state in Fig. 4 *a* demonstrate that at least two closed states are necessary to model the fast transitions in the channel, and an additional third closed state is needed for the extremely long closures (seconds long). This is evident in the macroscopic records as well, where the two time constants needed to fit the time course (Nicholson et al., 1993) demonstrate that there are at least three significant kinetic states (including the open state(s)) of the channel. On the other hand, a single exponential is sufficient for the pdf of the channel openings.

Further evidence for a second significant closed state comes from macroscopic records like those in Fig. 1. In these records, after application of a given potential for a certain time (400 ms or 4 s), the transjunctional voltage is reversed to the opposite polarity. Examination of the instantaneous current after such a polarity flip shows that the magnitude of these currents is always smaller than the instantaneous currents that arise when the voltage is stepped from 0 mV. This aspect of the data can be accounted for by another closed state.

The canonical model for hemichannel gating (Harris et al., 1981) has the kinetic scheme C–O. Based on the previous discussion, we propose an extension of this scheme with the following model:

$$O \underset{\beta}{\overset{\alpha}{\leftrightharpoons}} C \underset{k_u}{\overset{k_b}{\rightleftharpoons}} B \qquad (2)$$

for a hemichannel. Then the rate constants α and β that connect the O and C states are the analogs of the open and closed states in the conventional scheme. The ratio of the

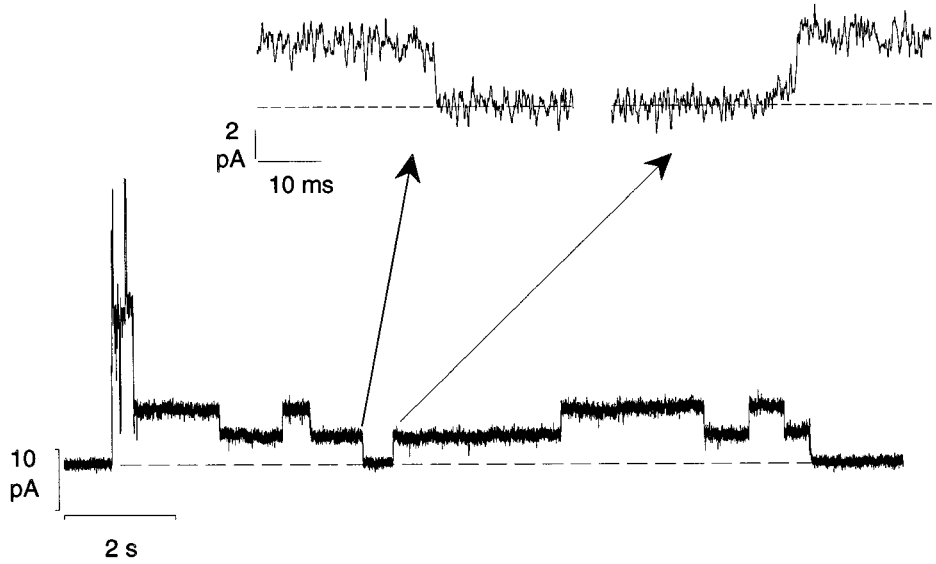

FIGURE 6 The Cx37 channel substate transits to complete closure at elevated salt concentrations (270 mM KCl at V_j of 40 mV). The inset shows the transitions to zero current (actually 0.2 pA or a conductance of 5 pS) in a faster time scale, with the data filtered at 1 kHz and sampled at 50 μs. The transitions seem to occur in a time less than 100 μs (dead time = 180 μs).

voltage dependence of these two rate constants is that which appears in traditional modeling of G–V curves. We will assume that their dependence on voltage will account for the fast gating, i.e., for that part of the gating that occurs in the vicinity of $V_j \approx 30$ mV. To account for the slow gating that occurs at large V_j, the rate constants k_b and k_u between the C and B states will be slower and, moreover, will be less dependent on V_j. Because these rate constants between B and C are slow, some of the hemichannels will be immobilized in the B state upon prolonged voltage steps and will open much more slowly upon voltage polarity reversal than hemichannels in the C state. This latter feature should then account for the drop in instantaneous current upon reversal of the voltage seen in the data (Figs. 1 and 5). All of the rate constants in the model are assumed to have an exponential dependence on voltage. Explicitly,

$$\begin{aligned} \alpha &= \lambda \exp(-A(V_j - V_0)) \\ \beta &= \lambda \exp(-B(V_j - V_0)) \\ k_b &= k_b^0 \exp(z_b V_j)) \\ k_u &= k_u^0 \exp(z_u V_j) \end{aligned} \tag{3}$$

In the model presented here, furthermore, the states denoted by C and B are assumed to have a conductance equal to the substate conductance G_s. This finite conductance of the supposedly closed state C (or B) is a feature of all gap junctional modeling (as implied by, e.g., Eq. 1). Such a peculiarity is necessitated by the observation that all gap junction channels have a nonzero steady-state macroscopic conductance at transjunctional voltages far removed from the half-activation voltage V_0. To account for the substate closures to complete zero at high voltage in Cx37 (see previous section), we could add more closed states with zero conductance connected to the B state. We have mimicked this by simply assuming that the apparent conductance of the B state tapers off with voltage to zero from a maximum equal to the substate conductance in accordance with the relation

$$G(B) = G_s * k_u/(k_u + k_b) \tag{4}$$

This reflects an equilibrium of the state B (the true conductance of which equals the subconductance G_s) with another closed state with zero conductance that does not otherwise enter explicitly into the model. The relationship assumes that the equilibrium constant between this anonymous closed state and the B state is then identical to the equilibrium constant between the C and B states.

The complete channel is modeled as two hemichannels, each of which follows the kinetic model in Eq. 2, though with opposing sensitivities to voltage. The complete kinetic scheme for the channel then has $3^2 = 9$ states, and the conductance of each of these 9 states is computed from the conductances of the corresponding kinetic states of the individual hemichannels (in series).

Published data on the same system (Veenstra et al., 1994) have demonstrated direct transitions between the open state and the ground or zero-conductance state. We have also observed similar transitions in the data that we have analyzed here. Such transitions are quite rare, however, and we have seen only five such transitions in the course of analyzing 40 min of data where there was exactly one channel in the patch. However, the linear model presented above precludes such direct transitions, with the open channel needing to traverse two subconductance states before closing completely to the ground state. We have not attempted here to account for this feature of the data because of the low frequency of events that pertain to this point. Nevertheless, it would not be surprising if additional (closed) states or pathways are necessary for a full description of the channel.

There is another point that we wish to address before describing the results obtained from the model above. In their classical description of gap-junction gating, Harris et al. (1981) provided two descriptions of the data. The first is that the two (hemichannel) gates of the channel function independently, with each following a C–O scheme. Apart from extending this two-state scheme to a three-state model, we have adhered to this prescription of independence in Eq. 2. As noted above, this extension is needed to account for 1) two-exponential macroscopic kinetics, 2) the two time constants for the single-channel closed pdf, and 3) reduction of the instantaneous channel current on voltage polarity reversal. In a second model, Harris et al. (1981) proposed that the two gates need not act independently, denoting such a mechanism as a "contingent gating" model. They further proposed a specific mechanism for contingent gating, namely that an open gate cannot close unless its partner gate is also open. Although we cannot rule out contingent mechanisms in general, we can show that the specific realization proposed by Harris et al. (1981) does not explain the data that we present here. Namely, we may observe in Figs. 1 and 5 that there are instances where the currents elicited by an initial pulse to V_j and by a pulse to V_j from $-V_j$ do not intersect. A specific example is also shown in Fig. 7 *d* (the same as Fig. 7 *a* at 150 mV), where the lighter lines are the current traces when the polarity is reversed. As noted in the original paper, this specific contingent-gating model requires, however, that the two curves intersect. We will also note that more detailed modeling of the full contingent gating model of Harris et al. (1981) (along the lines presented below) shows that that model does not statistically fit the data as well as the model in 2 (results not presented here).

The three-state model allows for an analytic solution of the time course; this solution is presented in the Appendix. This enables rapid prediction of the change in current for an ensemble of channels with a given set of parameters. The square of the difference between the data and the fit was used as the value to minimize; the actual minimization (Levenberg-Marquardt optimization) through parameter variation was done by using the FDJAC subroutine from

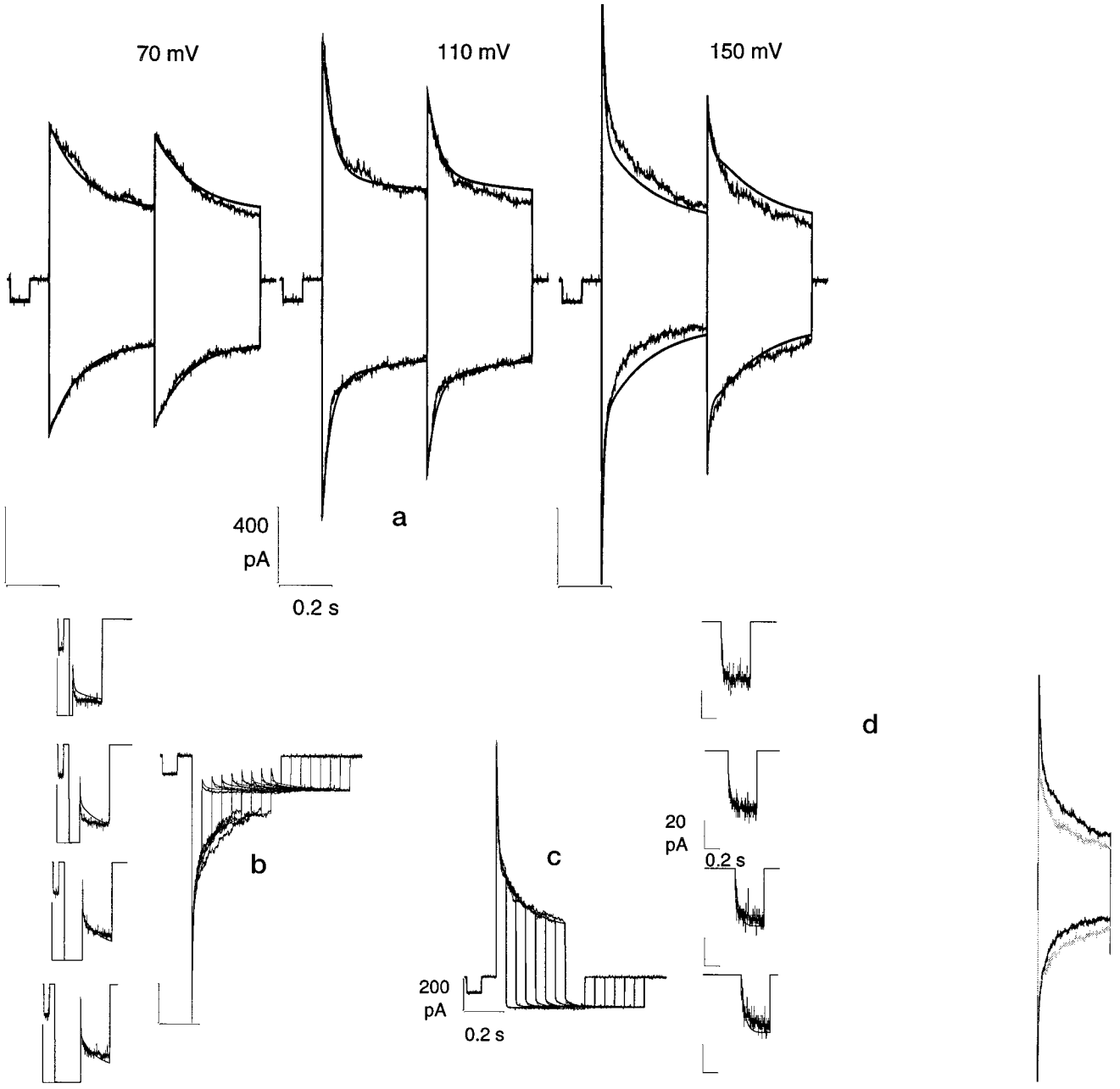

FIGURE 7 Fits of the model to the data. (*a*) Data acquired with the usual protocol, as described in the legend to Fig. 1 (1.8 mM $MgCl_2$). (*b* and *c*) Data from the same patch with a different protocol; the potential was stepped to −150 mV (in *b*) or 150 mV (in *c*). After various times at this potential, the potential was stepped to 20 mV. These protocols allow a better estimation of the slow time constants of recovery (to the open state) of a hemichannel. The solid lines in both panels are the results of the best fits obtainable with the model. (*d*) A replot of the data in *a* at 150 mV; however, the traces upon polarity reversal (in *light lines*) are superimposed on the traces on the direct step. The contingent model requires that the two traces intersect for all polarities; this is not true of the top trace. The reason that the traces are not similar for the two polarities is due to a small offset.

LINPACK (Dongarra et al., 1988). Different initial parameter values were tried to ensure that the optimization program explored various parts of the complex parameter surface and did not get trapped in a local minimum. Although we cannot be sure that the resultant parameter values are indeed the global minimum, they represent the best fits to the data, and as Fig. 7 demonstrates, they seem to fit various aspects of the channel kinetics quite well.

Fig. 7 *a* shows the best fits of the macroscopic records overlaid with the original data (reproduced from Fig. 1 *b*). These records were obtained with the usual reversing protocol (defined in the legend to Fig. 1). Data obtained with a different protocol from the same pair are also illustrated in Fig. 7, *b* and *c*. In this protocol, the voltage was stepped to a high V_j for various times and then stepped back to a constant potential of ±20 mV. The rationale for this proto-

TABLE 1 Best fit parameters

	λ	A	B	V_0	k_b	z_b	k_u	z_u	G_s/G
110 KCl 0.08 $MgCl_2$ $n = 5$, 1 s	2.06 ± 1.14	0.17 ± 0.08	−0.045 ± 0.012	31 ± 2	0.5 ± 0.5	0.018 ± 0.003	7 ± 5.7	−0.01 ± 0.002	0.4 ± 0.08
110 KCl 10 $MgCl_2$ $n = 4$, 1 s	5.16 ± 1.45	0.18 ± 0.16	−0.051 ± 0.011	37 ± 2.5	1.24 ± 0.2	0.017 ± 0.002	7.9 ± 2.9	−0.0065 ± 0.003	0.4 ± 0.04
180 KCl 2 $MgCl_2$ $n = 4$, 10 s	2.08 ± 0.62	0.13 ± 0.1	−0.064 ± 0.016	36 ± 10	0.28 ± 0.08	0.018 ± 0.011	1.6 ± 0.9	−0.018 ± 0.013	0.41 ± 0.12

All values are shown as mean ± SD. n is the number of experiments for the particular condition.

col was to unmask the slow unbinding from the extended closed state B. Upon stepping to a small potential (20 mV), where the channel is mostly open, from potentials where some fraction of channels are in the state B, the increase in current to the steady state allows more accurate estimation of the backward rate constant k_u.

Results of such fitting to various data sets are shown in Table 1. The rate constants k_b and k_u from the C to the B state are both smaller and less voltage sensitive than the rate constants for the O–C transition, in accordance with the design of the model. The parameters that are statistically different from the low to the high Mg^{2+} concentration (at 110 mM) are λ, V_0, and z_u. In fact, increasing the Mg^{2+} concentration apparently increases V_0, but this is more than offset by the change in λ. This latter change reduces the activation energy barrier between the O and the C states (given by kT log(λ)) enough to decrease the latent time before the channel enters the long closed or B state. This is illustrated further in Fig. 8, where the two macroscopic hemichannel time constants of decay (as computed from the average model parameters in Table 1) are plotted (as lines) against V_j for both low and high Mg^{2+} in panels *a* and *b*, respectively. The reduction in λ is reflected in the lowering of both time constants at high Mg^{2+}; this change overwhelms the slight shift in the curve due to changes in V_0. We wish to note further that the asymmetrical Mg^{2+} records such as those shown in Fig. 5, *c* and *d*, were also fit by the parameters from the symmetrical records in Table 1.

The symbols in Fig. 8 are the time constants obtained by a fit of the data used in Table 1 to a sum of two exponentials and a baseline. This is a five-parameter fit; the parameters are the baseline amplitude and the amplitude and time constants of the two exponentials. The various parameters, but especially the three amplitudes, produced by such fitting will not have any consistency across various potentials in a single data set, and the resultant time constants will not have a unified interpretation, as contrasted to time constants from a kinetic model. Nevertheless, the long time constants from these free fits have a trend similar to the predictions of the model.

For 10-s-long records at 180 mM KCl, the parameters in Table 1 that are different (statistically) from their counterparts for shorter times are k_b and k_u. Because these particular rate constants reflect slow immobilization of the channel in state B, this is in accordance with the observation of

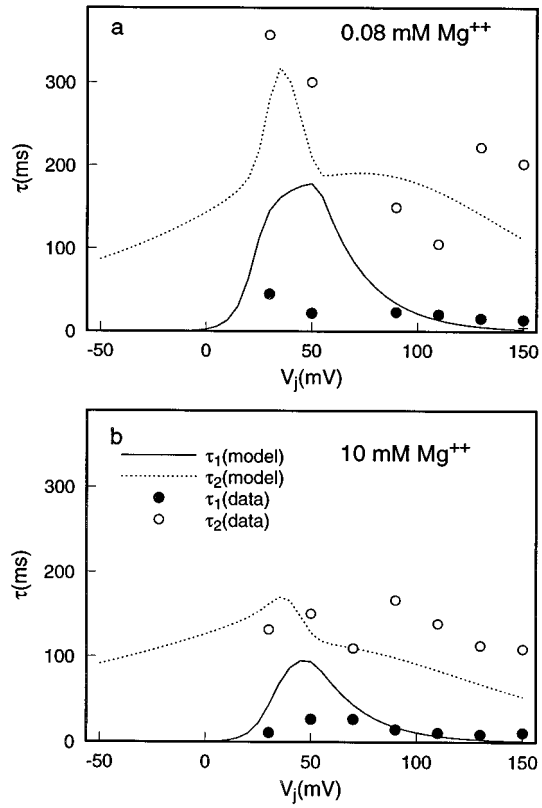

FIGURE 8 Predictions from the model of the dependence of the macroscopic time constants with voltage for two different concentrations of [Mg] at 110 KCl are shown in *a* and *b* by solid lines. The parameters for the predictions are taken from Table 1. The two solid lines are the two predicted time constants expected for the postulated three-state model. The filled and the unfilled symbols are the means (over data sets) of the short and long time constants obtained by fitting the data to a sum of two exponentials and a constant. Such fits are not constrained to be consistent across various potentials in any single data set (see text). The change from *a* to *b* in the predicted time constants with [Mg] is attributable primarily to the change in the parameter λ with [Mg]. The parameter λ is related to the height of the activation barrier between a closed (C) state and the open state of the model.

extremely long closures at high V_j's in single-channel records. We have also used the model parameters in Table 1 (at 180 mM) to predict the single-channel open and closed rate constants by the methods given by Colquhoun and Hawkes (1983). The predictions of the model are the lines in Fig. 4 (*solid* and *long dashed lines* for the closed time constants, *short dashed line* for the open time). The most prominent disparity is that for the shorter closed times. The predicted fast closed time constants rise steeply with voltage, as contrasted with that observed, which has a component that is roughly constant both in duration (10 ms) and in weight contributed to the closed pdf (0.8–0.9) in the range $15 \leq V_j \leq 30$ mV. Accounting for the discrepancy in the brief closures clearly requires an additional closed state, perhaps connected directly to the open state, as in models of the Shaker channel (Sigworth, 1993). Indeed, adding a closed state (denoted by F) with a lifetime of 10 ms connected directly to the open state (with O to F rate of 1/(150 ms)) yields a prediction for the closed single-channel pdf's that is close to that observed, both for the time constants and the weights.

Nevertheless, there is a difference between the voltage dependence of the single-channel pdf's and the macroscopic data. This difference is independent of the particular model used here. The open and closed times of the single-channel data in Fig. 4 do not show much variation over the range $15 \geq V_j \leq 25$ mV; this is different from the macroscopic data, which show deactivation at the higher end of this range ($G(30\text{ mV})/G(0) \sim 0.4$; see Fig. 2). We have no definite reason for this, but there are at least three possibilities: 1) As noted before in the section Microscopic Gating Data, long closures (10 s) are excluded from the closed pdf's. These closures would contribute to the macroscopic deactivation in 10-s records. However, collecting single-channel statistics on the long closures has proved difficult. 2) It is also possible that there is very slow depletion into the pipette of intracellular molecules of high MW that affect channel activity. 3) There is hetererogeneity or mode-shifting behavior in Cx37 channel gating, as has been noted for Cx43 (Brink et al., 1996). Such depletion may have effects that manifest themselves in long-duration single-channel records but not in macroscopic records. There is one possible method for elucidating the real reason for the differences in the data obtained by the two methods. This would involve repeated application of macroscopic protocols in one-channel patches and comparison of the averaged currents from these records to the macroscopic currents. The needed stability remains an experimentally difficult problem in the DWCP methodology.

We also tried a different hemichannel scheme of the form C–O–B but were unable to fit the kinetics well with this scheme, especially the slow macroscopic time constant and the behavior on voltage polarity reversal.

DISCUSSION

The gate in Cx37 is indifferent to the monovalent ions, has at least two closed states, and is influenced by [Mg]. Based on these observations, we have proposed a model of hCx37 gating that extends the canonical model of connexin gating (Harris et al., 1981). For Cx37, several investigators (Nicholson et al., 1993) have previously noted aspects of gating, most prominently in macroscopic records, that are inconsistent with the original model. Indeed, even for another connexin (rCx43), there is evidence (Brink et al., 1996; Banach et al., 1999) that the simple canonical model does not explain several facets of the data. The model that we propose is the simplest possible extension in that it has only three kinetic states for each hemichannel. It also takes explicitly into account the prominent substate that Cx37 resides in at low junctional potentials. The model makes some specific predictions, for example, that the change in kinetics with added [Mg] is predominantly due to a change in λ, which probably implies a binding site for Mg^{2+}, as opposed to a nonspecific screening effect that would only change V_0. At the least, the model presented here can be seen as more accurate than the canonical model in encapsulating the data from Cx37.

Magnesium concentrations in cells typically fall in the range of 0.2–2 mM (Birch, 1993). Because modulation of Cx37 gating occurs in this range, it is possible that there may be some physiological relevance to this effect. Such a hypothesis, of necessity, would need to be tested by methods that do not disrupt the internal cell milieu as drastically as does the whole-cell patch (e.g., a permeabilized patch).

APPENDIX

The time constants and the weights are solved by the usual formalism (Colquhoun and Sigworth, 1983). We present only the results. Define the auxiliary quantities

$$\Delta^2 = (\alpha + \beta - k_b - k_u)^2 + 4\alpha k_b$$

$$R = \frac{2(\alpha - k_b) + \beta - k_u}{\Delta + \alpha + k_b}$$

$$R' = \frac{\beta - k_u}{\Delta + \alpha + k_b}$$

$$S_0 = \frac{\beta k_b}{\beta k_b + \alpha k_u + \beta k_u} \tag{5}$$

$$S_1 = \frac{\beta k_u}{\beta k_b + \alpha k_u + \beta k_u}$$

$$S_2 = \frac{\beta(k_u + 2k_b)}{\beta k_b + \alpha k_u + \beta k_u}$$

$$S_3 = \frac{k_u(\beta + 2\alpha)}{\beta k_b + \alpha k_u + \beta k_u}$$

$$S_4 = (S_2 - S_3)/2, \quad S_5 = 1 - S_1, \quad S_6 = \frac{1}{2}\left\{1 + \frac{\alpha + k_b}{\Delta}\right\}$$

Then the eigenvalues are

$$(0, -(\alpha + \beta + k_b + k_u - \Delta)/2, \\ -(\alpha + \beta + k_b + k_u + \Delta)/2) \quad (6)$$

and the corresponding eigenvectors are

$$\begin{matrix} (k_u/k_b, & (\alpha k_u)/(\beta k_b), & 1) \\ (R', & (1 - R')/2, & -(1 + R')/2) \\ (1, & -(1 + R)/2, & -(1 - R)/2) \end{matrix} \quad (7)$$

The inverse eigenvectors are useful for computation and are given below:

$$\begin{matrix} (S_0, & S_0, & S_0), \\ S_6((S_2 - S_3)/2 + (1 - S_1)R, & S_2 - S_1R, & -S_3 - S_1R) \\ S_6(1 - S_1 + (S_2 - S_3)R'/2, & -S_1 - S_2R, & -S_1 + S_3R) \end{matrix} \quad (8)$$

The authors thank E. C. Beyer for providing the original transfected cells.

This work was supported by National Institutes of Health grant 31299 and a BASF fellowship to KB.

REFERENCES

Banach, K., S. V. Ramanan, and P. R. Brink. 1999. The high conductance of human connexin37 is determined by surface charges on the protein. *Biophys. J.* 76:000–000.

Birch, N. J. 1993. Magnesium and the Cell. Academic Press.

Brink, P. R., K. Cronin, K. Banach, E. Peterson, E. M. Westphale, K. H. Seul, S. V. Ramanan, and E. C. Beyer. 1997. Evidence for heteromeric gap junction channels formed from rat connexin43 and human connexin37. *Am. J. Physiol.* 97:C1386–C1396.

Brink, P. R., S. V. Ramanan, and G. J. Christ. 1996. Human connexin 43 gap junction channel gating: evidence for mode shifts and/or heterogeneity. *Am. J. Physiol.* 271:C321–C331.

Bukauskas, F., and R. Weingart. 1993. Multiple conductance states of newly formed single gap junction channels between insect cells. *Pflugers Arch.* 423:152–154.

Colquhoun, D., and A. G. Hawkes. 1983. The principles of the stochastic interpretation of ion-channel mechanisms. *In* Single Channel Recording. B. Sakmann and E. Neher, editors. Plenum Press, New York. 135–175.

Colquhoun, D., and F. J. Sigworth. 1983. Fitting and statistical analysis of single-channel records. *In* Single Channel Recording. B. Sakmann and E. Neher, editors. Plenum Press, New York. 191–263.

Dabrowski, A. R., and D. McDonald. 1992. Statistical analysis of multiple ion channel data. *Ann. Statist.* 20:1180–1202.

Dongarra, J. J., J. DuCros, S. Hammarling, and R. Hanson. 1988. An extended set of fortran basic linear algebra subprograms. *ACM Trans. Math. Soft.* 14(1):1–32.

Harris, A. L., D. C. Spray, and M. V. L. Bennett. 1981. Kinetic properties of a voltage dependent junctional conductance. *J. Gen. Physiol.* 77: 95–117.

Makowski, L. 1988. X-ray diffraction studies of gap junction structure. *Adv. Cell Biol.* 2:119–158.

Neyton, J., and A. Trautmann. 1985. Single channel currents of an intercellular junction. *Nature.* 317:331–335.

Nicholson, B., R. Dermietzel, D. Teplow, O. Traub, K. Willecke, and J. P. Revel. 1993. Divergent properties of different connexins expressed in *Xenopus* oocytes. *In* Progress in Cell Research: Gap Junctions, Vol. 3. J. E. Hall, G. Zampighi, and R. Davis, editors. Elsevier, Amsterdam, 3–14.

Reed, K. E., E. M. Westphale, D. M. Larson, H. Z. Wang, R. D. Veenstra, and E. C. Beyer. 1993. Molecular cloning and functional expression of human cx37. *J. Clin. Invest.* 91:997–1004.

Sigworth, F. J. 1993. Voltage gating of ion channels. *Q. Rev. Biophys.* 27(1):1–40.

Sigworth, F. J., and S. M. Sine. 1987. Data transformations for improved display and fitting of single-channel dwell time histograms. *Biophys. J.* 52:1047–1054.

Veenstra, R. D., H. Z. Wang, E. C. Beyer, S. V. Ramanan, and P. R. Brink. 1994. Connexin37 forms high conductance gap junction channels with subconductance state activity and selective dye and ionic permeabilities. *Biophys. J.* 66:1915–1928.

White, T. W., R. Bruzzone, S. Wolfram, D. L. Paul, and D. A. Goodenough. 1994. Selective interactions among the multiple connexin proteins expressed in the vertebrate lens: the second extracellular domain is a determinant of compatibility between connexins. *J. Cell Biol.* 125: 879–892.

Wilders, R., and H. J. Jongsma. 1992. Limitations of the dual voltage clamp method in assaying conductance and kinetics of gap junction channels. *Biophys. J.* 63:942–953.

Yeager, M., and B. J. Nicholson. 1996. Structure of gap junction intercellular channels. *Curr. Opin. Struct. Biol.* 6(2):183–192.